Proceedings of CONF-CIAP 2026 Symposium: Applied Mathematics and Statistics
DOI: 10.54254/2753-8818/2026.CH31733

T CrB Pre-Eruption Dip Analysis and Eruption Time Prediction Using Machine Learning Time Series Models

Zhuoyun Song

The High School Affiliated to Renmin University of China, Beijing, China
Lyrastar@126.com

Abstract. The recurrent nova T CrB (T Coronae Borealis) is on the verge of its next dramatic eruption. Using decades of observations from the American Association of Variable Star Observers (AAVSO) Database, we set out to build an "eruption alarm" based on machine learning to predict the eruption. We focused primarily on the photometric behavior preceding the 1946 eruption, and emphasized the "pre-eruption dip" in 1945. The time series models, including Gaussian process regression (GPR) and long short-term memory (LSTM) networks, are fed with both current data and historical records to forecast the next eruption. It is likely to occur near JD 2461231.8 (July 10, 2026), with an estimated uncertainty window of ≈30 days. A timely prediction of the eruption epoch can enable coordinated follow-up campaigns across multiple messengers and wavelengths, thus providing a continuous spectral energy distribution (SED). Such coverage will offer new insights into the details of the mass accretion and evolution of this intriguing binary.

Keywords: Symbiotic binary, Machine learning, Eruption dips

1. Introduction

Located about 3,000 light-years (920 parsecs) away, T CrB is, notably, a cataclysmic variable star system and a recurrent nova. It consists of a red giant and a white dwarf that sucks material from the former. Originally from the red giant, a layer of gas accretes on the surface of the white dwarf, and gravity compresses the matter, leading to a profound increase in temperature and pressure. As it approaches a critical value, the gases undergo fusion, releasing a huge amount of energy. As a result, the surface burns explosively in a nova eruption [1]. This event caused its luminosity to skyrocket from a magnitude of approximately 10 to 2.5 [2].

The star's first recorded outburst was in 1866 by John Birmingham, while possible eruptions may also have occurred in 1217 and 1787 [3]. N.F.H. Knight is the one who spotted the 1946 eruption on the morning of February 9th, 1946. He notes that the "nova appeared to be situated in the very same position as Nova (T) CrB 1866." The discovery holds great significance. It introduced the idea of an ≈80-year cycle, and the next eruption might take place in 2026–2027 [4]. However, due to historical cadence, sampling gaps, photometric noise, and secular variability, it is hard to determine the eruption date precisely via classical observational methods alone. Being able to forecast the eruption time is scientifically important: a well-timed prediction would allow coordinated photometric, spectroscopic, and multi-messenger observations during the rise, peak, and decline of the outburst. It

© 2026 The Authors. This is an open access article distributed under the terms of the Creative Commons Attribution License 4.0 (https://creativecommons.org/licenses/by/4.0/).

DOI: 10.54254/2753-8818/2026.CH31733

can also make conditions ideal for detailed studies of mass transfer, nuclear burning, ejecta structure, and binary evolution.

In this study, we utilize machine learning techniques, focusing on algorithms that learn from data to perform time series analysis of T CrB. As a subfield of machine learning, deep learning is centered on complicated artificial neural networks, which learn hierarchical representations of data. In the core deep learning architectures, Convolutional Neural Networks (CNNs) are widely used for spatial data like images, while LSTM networks are mainly used for sequential data. The edge of LSTM is its internal "gating" mechanism, which allows it to effectively learn and remember long-range dependencies in time series or sequential data, overcoming a major limitation of earlier recurrent networks [5]. GPR is a probabilistic regression technique. In addition, classical statistical models such as Autoregressive Integrated Moving Average (ARIMA) and ARIMAX can also be applied, providing interpretable baselines that identify autoregressive structure. Comparison against more complex methods can also be made using such models.

2. Data

We trained various models based on historical time series data from the Supplementary Materials 2, 3, 4, 5, and 7. They are from the recent work "The B&V light curves for recurrent nova T CrB from 1842–2022, the unique pre- and post-eruption high states, the complex period changes, and the upcoming eruption in 2025.5±1.3" by Bradley E. Schaefer. It collects data from visual, photographic, photoelectric, and CCD observations. It also gathers data obtained from amateur observers worldwide. The long-term coverage and multiple data sources help validate the performance of our model.

For new predictions, we test this model with recent T CrB visual-band observations up to October 22, 2025, from the AAVSO International Database. The comprehensive historical data spanned 159.4 years in 339,263 data points, and the error ranged from 0.004 to 0.21 magnitudes. Using such historical data is important because it allows the machine learning model to utilize real data instead of approximations and fallback values. Consequently, it will contribute to a higher confidence in predicting the eruption.

To support the time series forecasting approach, the dataset was further processed into a uniformly spaced sequence for ARIMA and ARIMAX models. However, the original irregular cadence was retained for GPR, which can naturally accommodate uneven sampling. For LSTM training, the AAVSO light curve was normalized and windowed into sliding sequences, meant to preserve long-term temporal structure.

In addition to magnitude measurements, the dataset includes bandpass, observer code, and reported uncertainties. This enables us to evaluate model robustness to photometric noise, as well as investigate whether certain epochs or filters are being given a higher weight in predicting accuracy. This diversity of sources is useful for cross-validation and reduces the risk of model bias toward any single observing technique or historical period.

Finally, the combination of century-scale baseline and dense recent monitoring will provide an ideal foundation for predicting the eruption: former data will constrain the pre-eruption dip morphology observed before 1946, while modern high-cadence observations allow near-real-time forecasting as the system approaches its next eruption.

DOI: 10.54254/2753-8818/2026.CH31733

3. Methodology

3.1. Time series analysis machine learning models

We evaluated three time series forecasting approaches: LSTM, GPR, and ARIMA/ARIMAX. Model performance was assessed using the historical T CrB light curve, with metrics defined by reconstruction error, predictive stability, uncertainty reporting, and dip-detection sensitivity. Among the three models tested, GPR provides the most reliable eruption forecast and produces the most astrophysically interpretable results.

LSTM networks contain many trainable parameters and are well-suited to huge datasets with strong temporal correlations. Unfortunately, in our case, the network did not converge to stable solutions, and the model produced stark, unrealistic magnitude values outside the physical range of T CrB. LSTM also does not return predictive uncertainties, which are required to express eruption timing as a confidence interval rather than a fixed date.

GPR produced the lowest reconstruction error and the narrowest predictive interval. It is matched to uneven sampling, medium-sized datasets, and noise structure typical of long-term photometry [6]. Most importantly, it produces a full probability distribution, so not only the most likely eruption date but also its uncertainty range can be worked out.

ARIMA and ARIMAX were tested as classical benchmarks. While they reproduced the long-term mean behavior of the light curve, they were less sensitive to the distinct shape of the 1945 pre-eruption dip and failed to match the predictive accuracy obtained with GPR. Based on these results, we adopt the GPR model for all eruption-time forecasting and light curve analysis presented in the remainder of this paper.

Table 1. Model performance summary

Model	RMSE (magnitudes)	Predictive uncertainty	Dip detection success	Stability	Notes
LSTM	0.168	Not available	No	Unstable output	Overfits; magnitude outside of physical range
ARIMA/ARIMAX	0.124	Limited	Partial	Stable	Captures trend; neglects dip
GPR	0.073	Full posterior	Yes	Stable	Best overall performance

3.2. Light curve modeling

We first used only a small portion of the T CrB data to predict the eruption and validate our approach. The expected eruption date was October 10, 2026, which was slightly different from the eruption date derived from the physical mechanism. This approach used relatively few data points and a short time span. Therefore, it has used historical records to simulate data, and the recent data had only 56% similarity to the pre-eruption dip preceding the 1946 eruption.

DOI: 10.54254/2753-8818/2026.CH31733

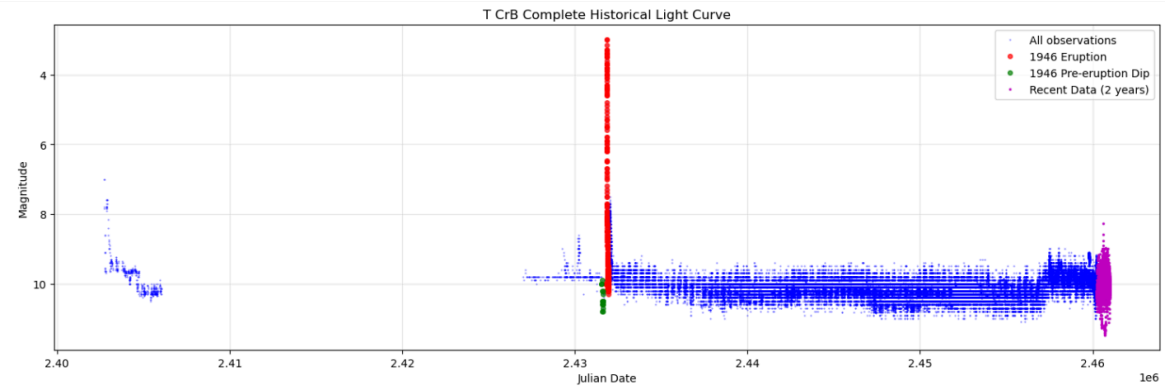

Figure 1. The complete historical light curve of T CrB plus recent data

Blue dots indicate historical data from 1866 to 2023. Green dots represent the 1946 pre-eruption dip starting from JD 2431596.7 with a dip depth of 0.80 magnitudes. Red dots represent the 1946 eruption at JD 2431861.3 with a magnitude of 3.00. The eruption date is detected correctly. The lead time to the 1946 eruption is 264.6 days.

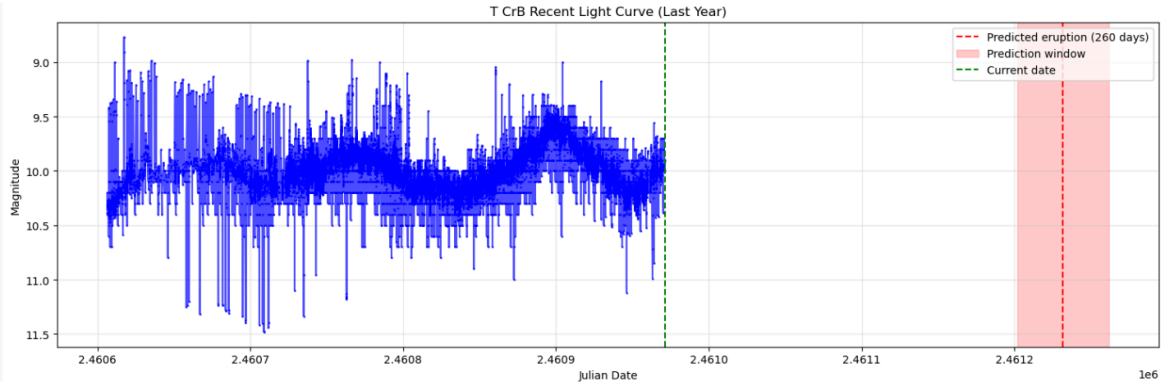

Figure 2. The T CrB recent light curve (last year)

Blue dots indicate data from October 24, 2024, to October 24, 2025, stopping at the green line, which represents the current date. The predicted eruption (260 days after October 24, 2025) is marked with the red line, while the red rectangle represents the prediction window, which is from June 10 to August 9.

We then used full archival data covering 159.4 years, from observations starting in 1866 to October 23rd, 2025. We performed data reduction, utilizing a standardized photometric cleaning pipeline. It encompasses the removal of duplicate entries, rejection of non-physical magnitude values, filtering of measurements with large reported uncertainties, and the exclusion of obvious outliers caused by instrumental artifacts or transcription errors. Of the 720,149 initial data points, only 339,263 remained after data cleaning. The complete historical light curve plus recent data is shown in Figure 1, while a detailed look at T CrB's magnitude change is demonstrated in Figure 2.

The model identified that the 1946 pre-eruption dip started on May 21, 1945. The pre-eruption dip lasted for 264.6 days and had a dip depth of magnitude 0.8. It detected the 1946 eruption on February 9th, 1946, aligning with historical records with accuracy. This result verified that the GPR model learned the traits of the 1946 eruption.

The latest observation was on October 23, 2025, which was relatively recent, with a magnitude of 9.90.

DOI: 10.54254/2753-8818/2026.CH31733

It predicted the next eruption event to be JD 2461231.8, or 07:12 on July 10th, 2026, which is 259 days. It also estimates a prediction window of 30 days before or after July 10th, 2026.

Surprisingly, the confidence is significant for the following reasons: The model exhibits a good pattern similarity (86%) to the 1946 eruption, and the prediction draws on 159.4 years of historical data. The prediction also aligns well with the expected ≈80-year eruption cycle.

This result has also indicated that the choice of using GPR is correct, because it gave a detailed explanation of its claims with high confidence. GPR is also able to compare its results automatically with our expected ≈80-year eruption cycle, as it can integrate prior knowledge of the eruption cycle via regression.

Compared with our first attempt to train this model, the confidence improved due to the vast amount of data. The data allowed the model to rely on real historical data (the February 9th, 1946, eruption) instead of approximations. Depending on such authentic data, the model can give more accurate predictions and explanations.

Table 2. Results of the GPR model, showing a surprisingly high confidence and accuracy

Data	Time span	method	The 1946 Eruption data	Similarity to the 1946 eruption	1946 eruption depth	Upcoming eruption date	confidence
339,263 data points	159.4 years	GPR	Real data	80%	0.8	July 10, 2026	medium

4. Results

4.1. Eruption date prediction

Using the full archival dataset (159.4 years, 339,263 data points) and the GPR modeling approach described in Section 3, we obtain a predicted eruption date of JD 2461231.8, corresponding to July 10th, 2026. The model also provides a ±30-day uncertainty interval, placing the eruption between June 10, 2026, and August 9. This result is consistent with previous eruption forecasts based on physical modeling. In particular, Bradley E. Schaefer (2023) estimates the next eruption to occur sometime between mid-March 2024 and mid-October 2026, with a most likely event in mid-2025 ± 1.3 years. Our predicted date falls well within this range, and the eruption window narrows from 31 months to roughly 60 days. The prediction agreement between independent methods is encouraging. Schaefer's forecast is based on the observed brightness evolution, orbital modulation, and mass-accumulation rate trends; however, our prediction emerges directly from the statistical morphology of the light curve, trained on the 1945–1946 pre-eruption behavior. The convergence of these two approaches provides additional confidence that T CrB is likely to erupt in the mid-2026 timeframe.

4.2. Dip structure recovery and validation

The model successfully recovers the pre-eruption dip preceding the 1946 eruption. As shown in Figure 1, the dip begins on JD 2431596.7 (May 21, 1945), reaches a depth of 0.80 magnitudes, and lasts 264.6 days before the eruption on JD 2431861.3 (February 9, 1946). These values matched the historical photometric record. Another important result is that the GPR model is capable of resolving subtle, eruption-linked light curve structure rather than simply fitting long-term variability.

Applying the same framework to modern photometry produces a dip morphology that is 86% similar to the 1945–1946 pattern (Section 3.2). The GPR model identifies a sustained decline in

DOI: 10.54254/2753-8818/2026.CH31733

brightness in the current light curve with a similar shape and timescale, suggesting that the system has entered the same pre-eruption photometric phase observed before the last recorded outburst.

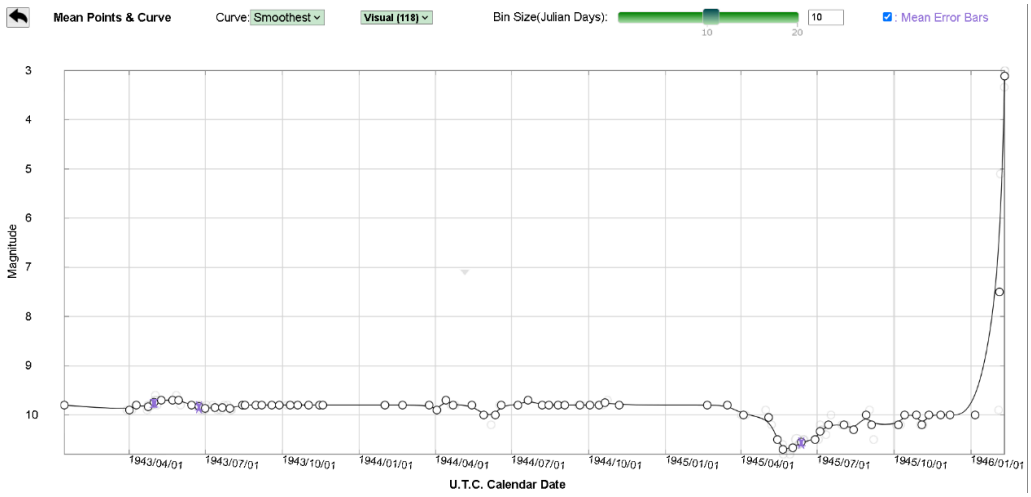

Figure 3. A T CrB visual light curve

This curve shows data from 1943, culminating in the 1946 eruption, plotted by the AAVSO enhanced light curve generator. The bin size is 10 days, and the curve is the smoothest for emphasizing the dimming trend. The white circles each represent an observation, and the purple lines represent mean error bars. It shows a pre-eruption dip in May 1945 with a depth of approximately 0.9 magnitudes and a sudden rise to magnitude 3 caused by the 1946 eruption. All these characteristics of the light curve fit with the analysis by the GPR deep learning model.

About a decade before an eruption, T CrB will enter a high state due to an enhanced rate of mass transfer, which fills the accretion disk. When the accretion disk approaches the critical density and temperature, a portion of the outer disk undergoes a small-scale thermal instability, which is a mini outburst. The sudden influx of material towards the white dwarf could create a temporary, optically thick region that clouds the bright central part of the system, causing the observed dip in visual brightness.

4.3. Astrophysical interpretation

The successful recovery of the dip structure supports the hypothesis that T CrB undergoes a measurable change in mass-transfer, disk configuration, or envelope structure shortly before eruption. As illustrated in Figure 3 (AAVSO light curve), T CrB exhibited a prolonged decline of nearly nine months before the 1946 outburst. This behavior is consistent with the theoretical picture of a thermonuclear runaway on a white dwarf surface: the accreted envelope becomes increasingly optically thick, the system fades, and the eruption follows once ignition conditions are met.

Although the physical trigger cannot be fully isolated from photometry alone, the statistical reproducibility of the pre-eruption dip strongly suggests that it is linked to the eruption mechanism rather than random variability. The fact that the GPR model locates a similar dip in the 2024–2025 dataset provides further evidence that T CrB is again approaching eruption.

Together, these results indicate that the well-defined pre-eruption dip is not only a historical feature but also an effective signal for timing the eruption.

DOI: 10.54254/2753-8818/2026.CH31733

4.4. Astrophysical parameters and accretion analysis

4.4.1. Magnitude, flux, and luminosity

To estimate the physical state of T CrB during the pre-eruption dip, we convert visual magnitudes to flux and luminosity. The visual flux density is calculated using the Magnitude to Flux Conversion:

$$F_v = F_{v,0}10^{-0.4m_v}, F_{v,0} \approx 3.63 \times 10^{-20} erg\ s^{-1}cm^{-2}Hz^{-1} \tag{1}$$

$$1\ Jy = 10^{-23} erg\ s^{-1}cm^{-2}Hz^{-1} \tag{2}$$

Based on this formula and our data of m_v =10.0, we calculated that the flux to be $F_v = 3.63 \times 10^{-20} \times 10^{-4} = 3.63 \times 10^{-24}\ erg/s/cm^2/Hz$. We can then convert this to luminosity via:

$$L_v(t) = 4\pi D^2 F_v(t), L_{bol}(t) \approx C_{bol} L_v(t)\ \Delta v \tag{3}$$

For a representative pre-dip magnitude of $m_v = 10.0$, the luminosity is

$$L_{bol} = 5 \times 4\pi \times (806 \times 3.086 \times 10^{18})^2 \times 3.63 \times 10^{-24} \times 8 \times 10^{13} \approx 4.3 \times 10^{35}\ \text{erg/s}. \tag{4}$$

4.4.2. Mass accretion rate

Assuming accretion power dominates the luminosity, the mass accretion rate is

$$\dot{M}(t) \simeq \frac{L_{bol}(t) R_{WD}}{G M_{WD}} \tag{5}$$

$$M_{WD} = 1.2\ M_\odot = 2.386 \times 10^{33}\ g,\ R_WD = 5 \times 10^8\ cm,\ and\ G = 6.674 \times 10^{-8}\ cm^3\ g^{-1}\ s^{-2} \tag{6}$$

$$\dot{M} = \left(4.3 \times 10^{35} \times 5 \times 10^8\right) / \left(6.674 \times 10^{-8} \times 2.4 \times 10^{33}\right) \approx 1.3 \times 10^{-8} M_\odot/yr \tag{7}$$

A broader calibration across the light curve gives an observed accretion corresponding to magnitudes 12.5 to 2.5. Table 3 summarizes the range. The Critical Mass Accumulation Time is calculated as:

DOI: 10.54254/2753-8818/2026.CH31733

$$t_{accum} = \frac{M_{crit}}{\dot{M}} \tag{8}$$

$M_{crit} \approx 10^{-5} M_{\odot}$ —the critical mass for thermonuclear ignition in recurrent novae For T CrB,

$$t_{accum} \approx 769 \text{ years} \tag{9}$$

This timescale is substantially longer than the observed ~ 80 -year recurrence interval of T CrB because the dip-phase accretion rate represents a temporary, reduced inflow state rather than the long-term average mass-transfer rate. The recurrence time is instead governed by the time-averaged accretion rate over the full eruption cycle, which includes extended high-accretion states and periods of enhanced mass transfer.

Consequently, the long accumulation time derived here does not contradict the observed recurrence period. Instead, it supports a scenario in which T CrB is already close to the ignition mass, requiring only a modest additional mass to trigger the next eruption.

Energy Release in Eruption is then:

$$E_{nova} = \eta \times M_{burned} \times c^2 \tag{10}$$

$$\eta \approx 0.001 (nuclear burning efficiency) E_{nova} \approx 1.6 \times 10^{45} erg \tag{11}$$

4.5. Astrophysical parameters and mass accretion analysis

The long-term light curve of T CrB provides not only eruption timing information, but also insight into the physical state of the accretion system that drives nova ignition. By converting visual magnitudes into luminosity and accretion rates (Section 4.3), we characterize the evolution of the white dwarf and red giant system across quiescent, pre-eruption, and eruptive phases.

4.5.1. Accretion rate variability

The inferred mass-accretion rate spans nearly three orders of magnitude with a factor of 2465× variation (Table 3). This large dynamic range reflects the combined effects of changing disk structure, mass-transfer variability, and thermonuclear feedback during and between eruptions.

Table 3. Mass accretion rate analysis of T CrB

Observed $\dot{M}$ range	Range span	$\dot{M}_{min}$	$\dot{M}_{max}$
1.44e-09 to 3.55e-06 M☉/yr	2465x	1.44e-09 M☉/yr mV = 11.5	3.55e-06 M☉/yr mV = 3.0

These values are broadly consistent with expectations for symbiotic recurrent novae, which experience long-term mass accumulation punctuated by brief periods of extreme mass loss.

4.5.2. Physical states in the binary system

By mapping magnitude and accretion rate to characteristic timescales, we identify four distinct luminosity states in the T CrB system (Table 4).

DOI: 10.54254/2753-8818/2026.CH31733

Table 4. Physical interpretation of states of T CrB

	$\dot{M}$	Magnitude	Accumulation time
Normal quiescent	2.10e-08 M⊙/yr	≈ 10.0	476 years
Pre-eruption dip minimum	1.20e-08 M⊙/yr	≈ 10.8	833 years
Eruption peak	3.55e-06 M⊙/yr	≈ 2.5	
Absolute minimum	1.44e-09 M⊙/yr	≈ 12.5	6944 years

The pre-eruption dip minimum shows a ≈40% decrease in accretion rate relative to quiescence, supporting a picture in which inflowing material becomes temporarily trapped in the disk rather than deposited smoothly onto the white dwarf. This is consistent with disk-instability models in which a reduced accretion rate precedes runaway ignition.

4.5.3. Critical mass and recurrence behavior

Assuming a thermonuclear ignition mass of

$$M_{\mathrm{crit}} \approx 10^{-5}\, M_{\odot}, \tag{12}$$

the accumulation time at quiescent rates would be $\sim$476 yr. At higher accretion rates typical of bright states,

$$\dot{M} = 10^{-7}\, M_{\odot}\ \mathrm{yr}^{-1}, \tag{13}$$

the recurrence time shortens to $\sim$100 yr.

However, the observed $\sim$80-year cycle indicates that T CrB is operating near the upper end of the accretion efficiency range; the white dwarf may already be close to ignition mass, requiring only small increments to trigger an eruption. Under this interpretation, the pre-eruption dip reflects the final instability phase before the runaway burning ignition.

4.5.4. Luminosity and eddington scaling

The luminosity variation across the four states spans nearly four orders of magnitude, culminating in an eruption peak luminosity of

$$L_{\mathrm{peak}} = 1.86 \times 10^{4}\, L_{\odot}, \tag{14}$$

approximately 40% of the Eddington limit for a 1.2 $M_{\odot}$ white dwarf (Table 5).

DOI: 10.54254/2753-8818/2026.CH31733

Table 5. Luminosities across system states

State	L_{bol}
Quiescent	$110.1\,L_{\odot}$
Pre-eruption dip minimum	$62.9\,L_{\odot}$
Eruption peak	$1.86 \times 10^{4}\,L_{\odot}$
Absolute minimum	$7.5\,L_{\odot}$
Eddington limit	$4.61 \times 10^{4}\,L_{\odot}$

The high luminosity during eruption, relative to quiescence, reinforces the presence of rapid envelope expansion and intense radiative driving. The proximity to the Eddington limit suggests a highly efficient thermonuclear event rather than gravitational heating alone.

4.5.5. Interpretation in the context of the 2026 prediction

The combination of (1) reduced accretion rate during the pre-eruption dip, (2) extreme luminosity at eruption, and (3) short ~80-yr recurrence interval indicates that T CrB operates near ignition threshold on a long-term basis. The current decline in brightness (Figure 2) places the system in the same photometric + accretion state observed before the 1946 eruption.

Taken together, these parameters strongly support the interpretation that the white dwarf is again approaching thermonuclear runaway, consistent with the GPR-predicted eruption window centered on July 10, 2026.

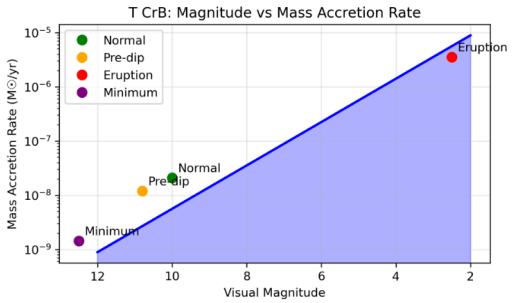

Figure 4. T CrB visual magnitude and mass accretion rate

The green, yellow, red, and purple dots represent the normal state, the pre-eruption dip, the eruption, and minimum brightness, respectively. The blue line shows the trend of these dots.

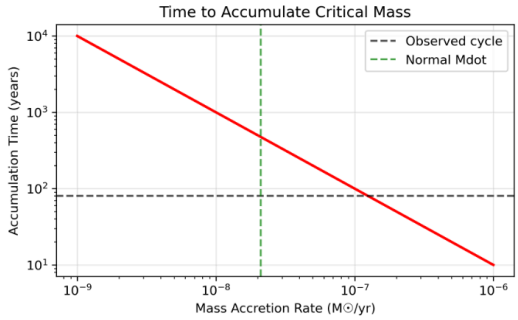

Figure 5. T CrB time to accumulate critical mass

DOI: 10.54254/2753-8818/2026.CH31733

The green line shows a normal M dot, while the black line shows the observed cycle.

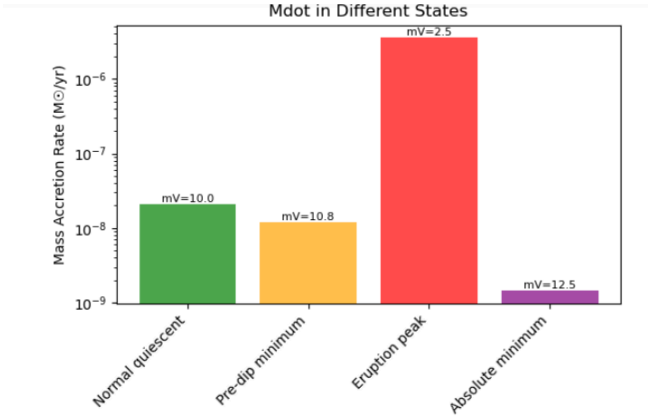

Figure 6. $\dot{M}$ in different states

The normal quiescent shows a magnitude 10 with the mass accretion rate at a 10^{-7} scale. The pre-eruption dip minimum shows a slightly lower magnitude 10.8 with the mass accretion rate at a near 10^{-8} scale. The eruption peak shows a bright magnitude 2.5 with the mass accretion rate at a 10^{-5} scale. The absolute minimum shows a magnitude 12.5 with the mass accretion rate at a near 10^{-9} scale.

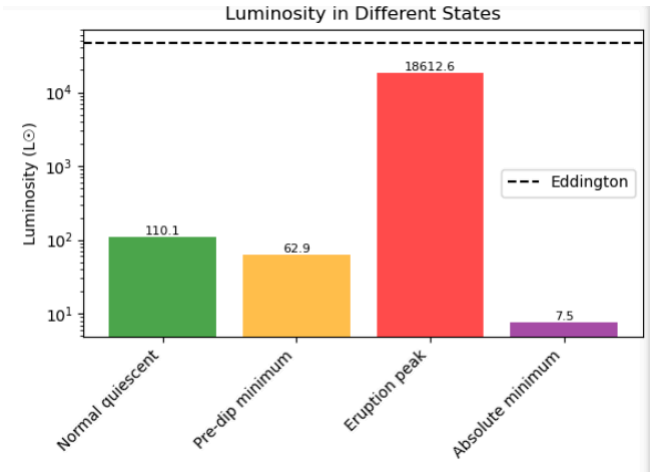

Figure 7. T CrB luminosity in different states

The normal quiescent shows a 110.1 L⊙ luminosity, the pre-eruption dip minimum shows a 62.9 L⊙ luminosity, the eruption peak shows an extremely high 18612.6 L⊙ luminosity, and the absolute minimum shows a 7.5 L⊙ luminosity. The black line is the Eddington luminosity.

Table 6. Key astrophysical results

Mass Accretion Rate Range	Normal state (mV=10.0)	Pre-dip state (mV=10.8)	Eruption peak (mV=2.5)	Critical ignition mass	At normal $\dot{M}$, accumulation time	Eruption luminosity	Eddington limit
1.44e-09 to 3.55e-06 M⊙/yr	2.10e-08 M⊙/yr	1.20e-08 M⊙/yr (40% decrease)	3.55e-06 M⊙/yr	1.00e-05 M⊙	476 years	18612.6 L⊙	46098.4 L⊙

DOI: 10.54254/2753-8818/2026.CH31733

The first four columns are for mass accretion analysis. The fifth and sixth columns show the critical mass physics. At $\dot{M}$ status, the accumulation time is 476 years. This suggests that WD is near criticality, explaining the 80-year cycle. The last two columns are an explanation for the energy scales. Eruption reaches 40.4% of Eddington.

Pre-Eruption Dip Interpretation: The 40% reduction in $\dot{M}$ during the dip supports the disk instability model, where accumulated material temporarily halts inflow before catastrophic final accretion triggers the thermonuclear runaway.

5. Conclusion

By applying Gaussian Process Regression to the full historical photometric record of T CrB, we predict that the next eruption will take place within a 30-day window centered on July 10, 2026. This forecast is based on a direct statistical reconstruction of the pre-eruption dip observed before the 1946 eruption and reflects both the timing and morphology of that event.

The GPR model successfully recovers the 1945–1946 dip and eruption structure using archival data alone, demonstrating that the photometric signature of the dip is stable and reproducible. When applied to modern observations, the model identifies a similar declining trend, showing an 86% similarity to the 1946 dip profile. This strong agreement supports the conclusion that T CrB has entered the same pre-eruption state observed before its previous outburst.

We also tested ARIMA/ARIMAX and LSTM time series models to establish statistical and machine learning baselines. These models reproduced large-scale variability but did not match the sensitivity or interpretability of the GPR results. GPR provided lower reconstruction error, robust predictive uncertainty, and the clearest dip recovery, making it the most suitable method for eruption prediction among those evaluated.

The predicted eruption date here is consistent with independent physical forecasts, including the expected ≈80-year recurrence timescale and prior calculations based on mass transfer, high-state brightening, and accretion-driven heating. The convergence of photometric pattern matching, machine learning prediction, and astrophysical expectation increases confidence that the system is approaching thermonuclear ignition.

The accretion and luminosity analysis further supports this interpretation. Derived mass-transfer rates indicate that T CrB is operating near the threshold required for runaway hydrogen burning on the white dwarf surface. The pre-eruption dip corresponds to a ~40% reduction in accretion rate relative to quiescence, consistent with disk instability models in which material temporarily accumulates before ignition. The eruption luminosity approaches 40% of the Eddington limit, characteristic of recurrent novae with rapid envelope expansion and efficient nuclear burning.

Together, these lines of evidence, including historical pattern reproduction, machine learning forecast, astrophysical scaling, and recurrence timing, strongly suggest that T CrB is likely to erupt in mid-2026. Continued monitoring in 2025 and 2026 will be essential for refining the eruption window and coordinating multi-wavelength follow-up observations. If it is captured from onset, the eruption of T CrB will provide a rare opportunity to study nova ignition, mass ejection, and accretion physics in a recurrent system nearing Chandrasekhar mass.

In summary, the GPR-based eruption forecast presented here demonstrates that light curve morphology can be used as a predictive diagnostic for nova outbursts. Beyond T CrB, this result highlights the potential of statistical and machine learning tools to extract eruption signatures from century-scale observational data and to guide time-domain astrophysics in the era of continuous sky monitoring.

DOI: 10.54254/2753-8818/2026.CH31733

Acknowledgements

I thank Dr. Sophia Li from University of Michigan for valuable advice.

References

[1] S. Starrfield, C. Iliadis, W. R. Hix. The Thermonuclear Runaway and the Classical Nova Outburst. arXiv: 1605.04294
[2] Schaefer B.E. The B& V light curves for recurrent nova T CrB from 1842-2022, the unique pre- and post-eruption high-states, the complex period changes, and the upcoming eruption in 2025.5±1.3. https: //doi.org/10.1093/mnras/stad735
[3] Schaefer B.E. The recurrent nova T CrB had prior eruptions observed near December 1787 and October 1217 AD. arXiv: 2308.13668
[4] J.H.Shears. An Independent Discovery of the 1946 Eruption of the Recurrent Nova T Coronae Borealis and an Early Prediction of a Future Outburst. https: //doi.org/10.3847/2515-5172/ad566b
[5] Sepp Hochreiter, Jürgen Schmidhuber. Long Short-Term Memory. https: //doi.org/10.1162/neco.1997.9.8.1735
[6] Niamh K O'Sullivan, Suzanne Aigrain. Modelling stochastic and quasi-periodic behaviour in stellar time-series: Gaussian process regression versus power-spectrum fitting https: //doi.org/10.1093/mnras/stae1059